

Comparison between common models of forces on oar blades and forces measured by towing tank tests

S Barré^{1,2} and J-M Kobus^{2*}

¹Ecole Nationale de Voile et des sports Nautiques (ENVSN), Saint pierre Quiberon, France

²Laboratoire de Mécanique des Fluides (LMF), Ecole Centrale de Nantes, Nantes, France

The manuscript was received on 5 February 2009 and was accepted after revision for publication on 22 June 2009.

DOI: 10.1243/17543371JSET43

Abstract: This paper describes the hydrodynamic forces on oar blades and compares measured data with common models: one model using a normal force coefficient and the other using drag and lift coefficients. The data were obtained from tests in towing tanks on blades at reduced scale (typically 0.7). The measurement device can reproduce oar movements and measure the six components of the hydrodynamic efforts. These tests provide a better control, precision, and repeatability than measurements on water. The experimental modelling leads to defining the oar strokes using only the maximum rotation rate and an advance number, which can also be defined as basic efficiency. These movements are simplified but remain representative of the main characteristics of the unsteady working of oars. The measurements show how the direction and zero-torque point influence instantaneous efficiency. They also show that the force evolution can be described using the maximum values of drag and lift coefficients. These depend on the unsteadiness, characterized by a parameter equal to the difference between the velocities of the two blade edges divided by the normal component of the velocity of the blade centre. This parameter, fully related to the advance number, can be considered as a reduced frequency.

Keywords: rowing, oar blade, hydrodynamic force, model, efficiency, measured data

1 INTRODUCTION

Rowing is a rather intricate problem of propulsion which involves many physical phenomena that span a large number of scientific fields such as mechanics, fluid mechanics, biomechanics, physiology, etc. The analysis of rowing performance requires knowledge in each field and in each subsystem that contributes to the whole system. However, it is difficult to apply this knowledge to improve performance because the subsystems are fully coupled and involve numerous parameters. The numerical simulation of rowing is now commonly regarded as a good means to understand and analyse the operation of the complete system of oars, rowers, and boat. The objective of the authors who use simulation is generally to quantify the influences of the operation parameters and to seek ways to optimize performance [1, 2].

The relevance of the optimization of the complete system depends on the accuracy of the models used to calculate the forces on each part of the system during the simulation. This requires a thorough study of the phenomena involved in oar propulsion, the hydrodynamics of the blade, the hydrodynamics of the boat, a biomechanics model of the rower, an analysis of the 'rowing technique', and particularly the displacement of the centre of gravity. All these points can be treated with advanced experimental techniques or with numerical tools.

The problem in the numerical simulation of rowing is that, when the kinematics of the rowers and oars are imposed, the instantaneous speed of the boat is not previously known. It is therefore difficult to calculate the propulsive forces of the oars with models whose coefficients depend on this speed. There is still much work to be done to produce a model that can provide to a simulator, at each moment, a precise value of the forces which load the oar blade, according to the state variables and the history of the flow. This will probably only be possible by using computational fluid dynamics (CFD) calculations on the

*Corresponding author: Laboratoire de Mécanique des Fluides, UMR CNRS 6598, Ecole Centrale de Nantes, 1 rue de la Noë, BP92101, Nantes, 44321, France.

email: Jean-Michel.Kobus@ec-nantes.fr

blade, which will be completely coupled with the mechanical part of the simulator. However, the calculations will be so computationally expensive that they will only be used as a reference case and not for the purpose of optimization. An alternative method, allowed by simulation, is to make the coefficients converge towards adequate values over several cycles. When searching for a good technique to obtain convergence, it is possible to use parametric models. This method is explored in this paper which focuses on the modelling of the hydrodynamic propulsive force on oar blades.

The flow around oar blades involves pressure effects, added mass, vortex, free-surface effects, etc. Even though progress in numerical methods has enabled the use of CFD codes to study the flows around blades, accurate measured data are still needed to validate the numerical results [3]. Thus, an experimental approach is still appropriate to evaluate the forces induced on blades by such a complex flow.

Although they are directly correlated to the performance of the system, measurements on water of the forces applied on oars do not allow all of the parameters to be controlled and are thus not very precise or repeatable. Tests in the laboratory provide a better control of parameters but require a simplification of the real operating system depending on the technical means available. Some attempts have been made in this field: Doi *et al.* [4] tested real oars in a towing tank at constant speed and incidence; Caplan and Gardner [5] tested blades at quarter scale in a water-circulating flume at constant incidence; Kinoshita and Kobayashi [1] also tested oar blades at reduced scale in a water-circulating flume, but the blades were rotated around their centre in the steady flow. Their measurements clearly highlight the influence of the unsteadiness of the phenomenon. In this paper a special dynamometric device is used to test oar blades in a towing tank. This device enables a more realistic movement to be applied to the oars [6].

2 METHOD

The purpose of this investigation is to highlight the unsteady effects on flow behaviour and to understand which factors affect propulsive efficiency. It is also an opportunity to verify some current assumptions about the direction of the hydrodynamic force and the position of the point where the force acts. The experimental data are compared with the models currently used in rowing simulation. The experimental results that are presented here were obtained from systematic tests in a towing tank with dimensions of 145 m × 5 m with a depth of 3 m that is located at the Laboratoire de Mécanique des Fluides (LMF), Ecole Centrale de Nantes.

2.1 Experimental approach

The proposed approach is to reproduce the movements of blades as accurately as possible in a towing tank. This technique separates the propulsive device (the oar) from the motor (the oarsman) and from the boat, as is done for propellers. To achieve this, the LMF has designed an apparatus for testing models of blades at reduced scale and oars at real scale. The system generates a simplified rowing stroke but with good control of the parameters and accurate reproducibility. In order to avoid a complex mechanism, the blades always remain in the water. To limit the consequences of this feature, it is possible to impose a movement (called a neutral movement) to minimize the forces on the blades before the catch angle of the real stroke. This technique introduces supplementary parameters such as the neutral movement duration and the transition phase duration (catch). In order to perform systematic tests, simplified movements were also defined using only two kinematic parameters specified under efficiency considerations, as described later.

2.2 Experimental device and procedure description

2.2.1 Experimental device

The device is a six-component dynamometer equipped with a servo motor of high specific power and with a mechanism that reproduces accurately and repetitively the movement of the oar blade in the water (Fig. 1). The rate of rotation is reduced by a gear box and two pulleys with a timing belt. A numerical controller makes the motor conform to a

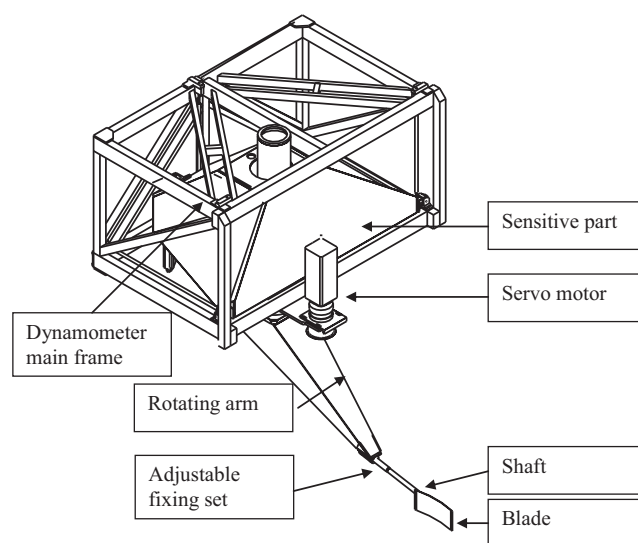


Fig. 1 View of the measurement device. The rotating arm, the servo motor, and the gear box are fixed on the sensitive part of the six-component dynamometer

given displacement or speed value. The motor and the transmission mechanism are directly attached to the dynamometer in order to eliminate the influence of the transmission efforts and to measure the hydrodynamic forces on the blade. The device is fixed on the towing tank carriage and the speed of translation is constant during the stroke. From the literature and measurements on water, it was deduced that the amplitude spectrum of forces has no significant value beyond 7 Hz so the device is designed to obtain natural frequencies over 15 Hz. For this purpose, the sensitive part of the dynamometer and the rotary arm are built with carbon fibres and resin. The blades are attached to the rotary arm by a fixing set which allows the adjustment of the external lever, the inclination of the oar shaft, and the angle of the blade to the vertical direction. The immersion adjustment is set by shifting the dynamometer support up and down. With this arm, a scale of 0.7 was chosen for the oar blades. The blade shafts are very short and are made of monolithic carbon to obtain a great rigidity.

2.2.2 Experimental procedures

The measurements are processed as follows: the device gives eight outputs: six from the force transducers of the dynamometer, two others from the angular position and the velocity of the servo motor. These signals are sampled and stored. The six components of the forces, in the dynamometer frame of reference, are calculated at each time sample using a calibration matrix. Next they are filtered to eliminate noise and forces induced by the vibrations of the dynamometer. Angular position and velocity are also sampled and filtered. Finally, corrections are applied to eliminate the inertial efforts of the rotary parts and the induced aerodynamic efforts. All the test procedures are described in detail in Leroyer *et al.* [3], Barré and Kobus [6], and Barré [7].

2.3 Significant parameters for experimental modelling

2.3.1 Efficiency parameter

Since the oar is isolated from the whole rowing system, the instantaneous efficiency of the propulsive device can be defined as the ratio of the useful power to the delivered power

$$\eta = -\frac{F_x V_b}{M_z \dot{\theta}} \quad (1)$$

where M_z is the component of the hydrodynamic torque applied about the vertical axis of unit vector e_{zO} . The point A (see Fig. 2), where the hydrodynamic force F acts on the blade, is not known nor is the value of the pure moment m which appears because of the rotation of the blade. M_z can be formulated by

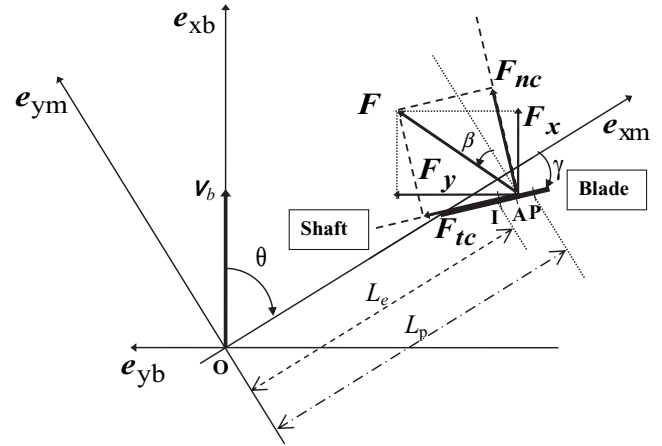


Fig. 2 Definition of characteristic points and angles

$$M_z = M_O \cdot e_{zO} = (OA \times F + m) \cdot e_{zO} = (OP \times F + M_P) \cdot e_{zO} \quad (2)$$

If P is chosen in order to have $M_P \cdot e_{zO} = 0$ then

$$M_z = (OP \times F) \cdot e_{zO} \text{ and } m = AP \times F \quad (3)$$

The position of the point P moves during the stroke.

If I is the reference point, generally placed at the centre of the blade, let us note $Le = \overline{OI}$ the distance of I to e_{zO} and L_{ip} the algebraic distance \overline{IP} projected on the horizontal plane. Assuming that neither the friction and suction effect nor the flexion of the shaft is affecting the torque M_z , this can be written as

$$M_z = (L_{ip} + Le)F_n \quad (4)$$

and $M_z = (Le + L_{ip})(F_y \cos \theta - F_x \sin \theta)$ by introducing the components of the hydrodynamic force into the dynamometer axis.

The efficiency is then defined by

$$\frac{1}{\eta} = \frac{M_z \dot{\theta}}{F_x V_b} = \frac{\dot{\theta}(Le + L_{ip})}{V_b} \left(\frac{F_y}{F_x} \cos \theta - \sin \theta \right)$$

If the angle of the hydrodynamic force with the perpendicular to the shaft is noted β , then

$$\frac{F_y}{F_x} = -\frac{1}{\tan(\beta + \theta)}$$

and hence

$$\eta = \frac{V_b \sin \theta}{Le \dot{\theta} (1 + L_{ip}/Le)} \left(1 + \frac{\tan \beta}{\tan \theta} \right)$$

As L_{ip} is always small compared to Le , an approximate efficiency expression is

$$\eta = \left(\frac{V_b \sin \theta}{Le \dot{\theta}} \right) \left(1 - \frac{L_{ip}}{Le} \right) \left(1 + \frac{\tan \beta}{\tan \theta} \right) = \eta_0 \eta_p \eta_f \quad (5)$$

This expression of efficiency can be broken down into three parts:

- (a) basic efficiency depending only on the oar movement

$$\eta_0 = \frac{V_b \sin \theta}{Le \dot{\theta}}$$

- (b) efficiency coefficient depending on the position of the zero torque point

$$\eta_p = 1 - \frac{L_{ip}}{Le}$$

- (c) efficiency coefficient depending on the direction of the hydrodynamic force

$$\eta_f = 1 + \frac{\tan \beta}{\tan \theta}$$

2.3.2 Advance parameter

The hydrodynamic forces depend on the fluid characteristics, on the gravitational acceleration g (free-surface effects), and on the blade characteristics and working parameters (outboard lever, boat velocity, oar angular position, velocity, and acceleration). They have the general form $F = f[\rho, \nu, g, Le, V_b(t), \theta(t), \dot{\theta}(t), \ddot{\theta}(t), \dots]$. The efforts also depend on the history of the flow, especially in the second part of the stroke, when the blade passes through the fluid which it has already disturbed.

Because the motion is not steady, the non-dimensional coefficients that could describe the propulsion are not constants but will be related to time. The form of these parameters will depend on the relation between $\dot{\theta}(t)$ and $\theta(t)$. For systematic testing, a simple relation between $\dot{\theta}(t)$ and $\theta(t)$ was sought. To remain realistic, this relation is based on energy considerations and on observations of the real operation of oars.

As previously stated the efficiency of the oar stroke can be represented by its main component $\eta_0 = V_b(t) \sin \theta(t) / (Le \dot{\theta}(t))$. The tests in a towing tank impose a constant velocity V_b . As noted by Wellicome [8], the total efficiency reaches a maximum value if the instantaneous efficiency is constant. When measuring η_0 in real conditions with elite rowers (for example in Fig. 4), it can be observed that this parameter varies only slightly. Thus, a relation between the angular speed and the angular position which gives η_0 constant was adopted for systematic towing tank tests, i.e. $\dot{\theta} = K \sin \theta$ with $K = \dot{\theta}_{\max}$.

In the theory of propellers, the advance number is defined as V_b/nD (where n is the rate of rotation and D the diameter). It is representative of the incidence of incident flow on the blade. By analogy, $V_b/(KLe)$, which is also the kinematic efficiency component

η_0 , can be considered as an advance number. The movement of the oar blade being unsteady, this parameter does not represent the incidence but it characterizes the law of variation of the 'pseudo-incidence' of the flow on the oar blade (angle α). The pseudo-incidence is calculated arbitrarily at the centre of the blade and varies with θ during the stroke. The relation between α and θ is $\tan \alpha = (1 - 1/\eta_0) \tan \theta$ which is independent of K .

Figure 3 shows the evolution of the pseudo-incidence angle α according to the θ angle. It can be shown that $d\alpha/dt = K\eta_0/(1 - \eta_0)$ for $\theta = -90^\circ$. Thus, the higher K and η_0 are, the more the pseudo-incidence angle varies greatly at $\theta = -90^\circ$.

Figure 3 also shows how the normal and tangential components of the incident velocity vary with θ according to the advance number.

To conclude, in order to reduce the number of parameters, most tests in the towing tank were made with $\dot{\theta} = K \sin \theta$ for the oar rotation law. Consequently, systematic tests were performed for different pairs of parameters

$$K = \dot{\theta}_{\max} \quad \text{and} \quad \eta_0 = V_b/(K \times Le) \quad (6)$$

2.4 Derived non-dimensional parameter for the data analysis

2.4.1 Reduced frequency

In order to characterize the unsteadiness of the stroke, another non-dimensional number is defined which represents the velocity difference between the leading edge and the trailing edge of the blade divided by the normal component of the velocity of the centre of the blade. This number is expressed as a reduced frequency $f_r = c\dot{\theta}/V_n$.

Since $V_n = Le\dot{\theta} - V_b \sin \theta$, with the oar kinematic $\dot{\theta} = K \sin \theta$, f_r can be written as

$$f_r = \frac{c K \sin \theta}{Le K \sin \theta - V_b \sin \theta} = \frac{c}{Le} \times \frac{1}{1 - \eta_0} \quad (7)$$

This number does not depend on θ and is fully related to η_0 .

With the imposed kinematic, the time to rotate from $\theta = 0$ to $\theta = -\pi$ is theoretically infinite. Nevertheless, the characteristic time T to rotate between θ_1 and θ_2 is

$$T = t_2 - t_1 = \frac{1}{K} \ln \frac{\tan(\theta_2/2)}{\tan(\theta_1/2)}$$

If θ_1 and θ_2 are chosen to be significant angles with regard to the hydrodynamic forces during the stroke, the duration of the unsteady movement is then proportional to $1/K$. Then, the reduced frequency f_r has the form of a Strouhal number c/TU . It accurately represents the unsteadiness of the phenomenon.

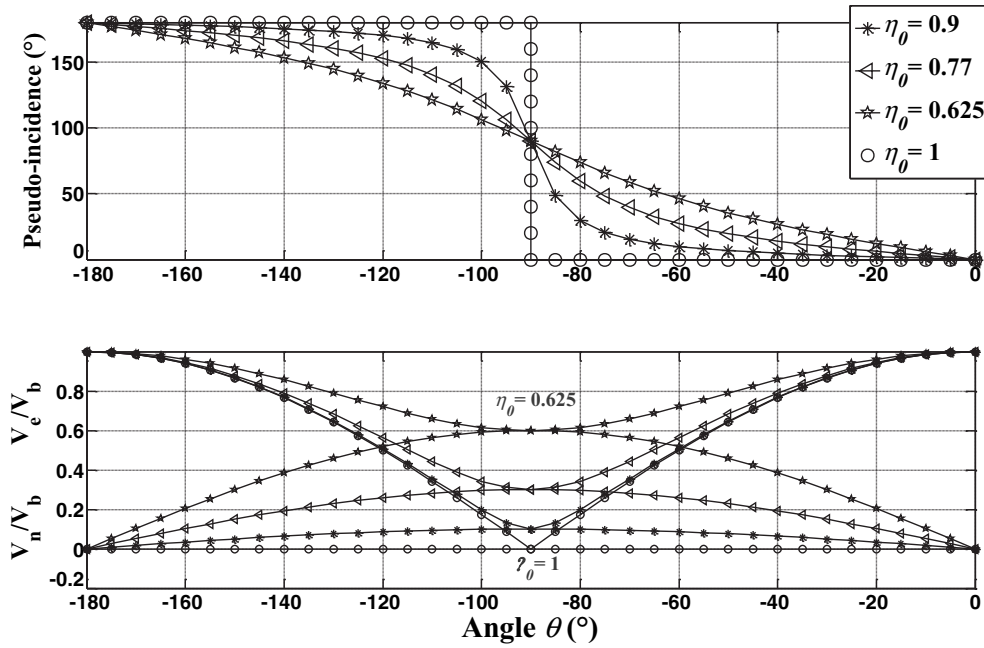


Fig. 3 Pseudo-incidence, normal, and tangential velocity at the reference point of the blade

Although the experimental conditions are different from those of Kinoshita and Kobayashi [1] (a rotation around the blade centre in a uniform stream), the approach of the reduced frequency is similar.

2.4.2 Froude number

To take into account the influence of the free-surface effects, a Froude number is adopted based on V_n the normal velocity of flow, which is the more significant component of the velocity according to the free surface disturbance. When calculating V_n/\sqrt{cg} it is found that

$$\begin{aligned} V_n/\sqrt{cg} &= (V_b \sin \theta - Le\dot{\theta})/\sqrt{cg} \\ &= V_b \sin \theta(1 - LeK/V_b)/\sqrt{cg} \\ &= \sin \theta KLe(\eta_0 - 1)/\sqrt{cg} \end{aligned}$$

This quantity depends not only on the two parameters of the modelled stroke but also on θ . Fr_n is chosen as the maximum value for $\theta = -90^\circ$

$$\begin{aligned} Fr_n &= KLe(1 - \eta_0)/\sqrt{cg} = Le(1 - \eta_0)/c \times K\sqrt{c/g} \\ &= K/f_r \times \sqrt{c/g} \end{aligned} \quad (8)$$

2.5 Choice of the parameters K and η_0 for model testing

The significant values of the parameters K and η_0 were evaluated with some *in situ* tests. During these tests, the oar position and the boat speed were measured to calculate the coefficient $K(t)$ and the advance number $\eta_0(t)$ with the relations $K(t) = \dot{\theta}/\sin \theta$ and $\eta_0(t) = V_b(t) \sin \theta/Le\dot{\theta}$.

Figure 4 shows an example of the results obtained with two stroke rates (18 and 36 str/min) for an elite rower on a skiff. It can be seen that η_0 varies slightly between $\theta = -35^\circ$ and $\theta = -110^\circ$ but $K(t)$ increases because $K(t) = V_b(t)/Le\eta_0$ and $V_b(t)$ increases during most of the real stroke. Notice that these results are also biased by the oar deformation during the stroke, which slightly modifies the velocity of the blade and the pseudo-incidence of the flow.

Nevertheless, to choose the range of parameter values for testing in the towing tank, it was considered that the significant values for η_0 vary from 0.6 to 0.8. For K , the significant values were chosen in the middle of the stroke between 2.5 and 3.5 rad/s because the Froude number (i.e. the free-surface effect) has the greatest influence around $\theta = -90^\circ$.

For the towing tank tests at reduced scale, the similitude must respect the advance number which gives the same relation between the swing angle θ and the pseudo-incidence α and the same reduced frequency f_r . Because of free-surface effects, the similitude also respects the Froude number. The Reynolds number cannot be respected. This partial similitude leads classically to

$$V_{b \text{ model}} = V_{b \text{ real}}\sqrt{e} \quad \text{and} \quad K_{\text{model}} = K_{\text{real}}/\sqrt{e}$$

with $e = Le_{\text{model}}/Le_{\text{real}} = c_{\text{model}}/c_{\text{real}} < 1$ being the scale.

The values of the coefficients K used for systematic tests at a scale of 0.7 will thus lie between 3 and 4.5 rad/s. The advance number values are between 0.6 and 0.8.

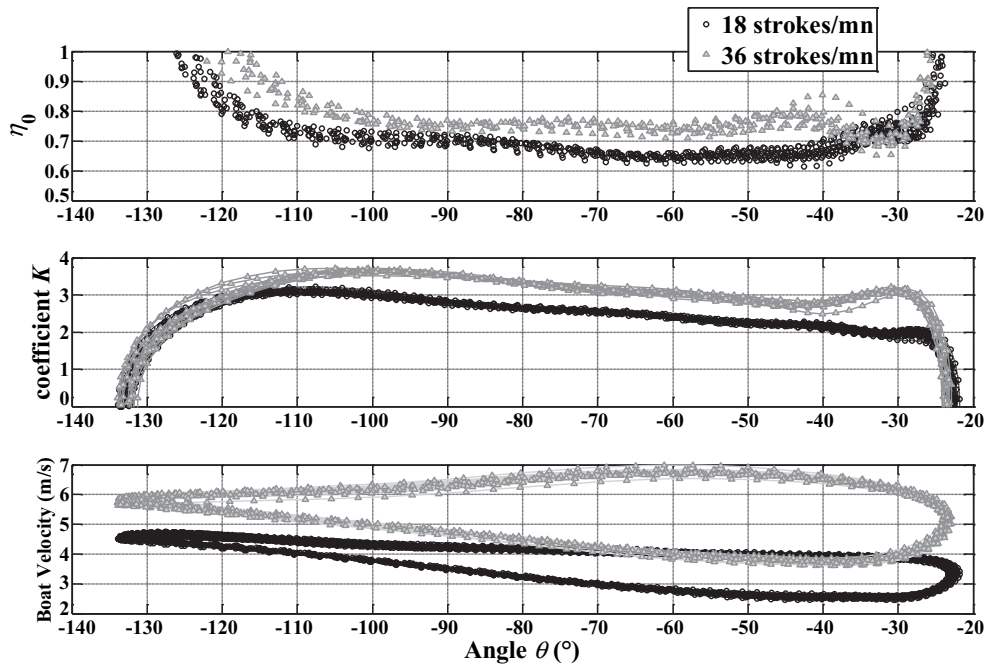


Fig. 4 Advance number $\eta_0 = V_b \sin \theta / Le \dot{\theta}$ and coefficient $K = \dot{\theta} / \sin \theta$ from tests on water

3 RESULTS AND DISCUSSION

The results presented here are based on the tests of two blades whose characteristics are given in Table 1.

The first oar blade (pal0bis) is a flat rectangle. The blade chord is aligned with the shaft. The second (pal1) is also rectangular but it has an identical transverse and longitudinal curvature, so this blade is called a 'spherical blade'. The blade chord has an angle of -5° to the shaft ($\gamma = -5^\circ$). All the blades have a thickness of 3.5 mm.

The shaft and blade flexions are assumed to be negligible. During the tests, the blades are vertical and their upper edges remain at the level of the still free surface of the water.

The results presented in this section are restricted to four cases: $K = 3$ rad/s and $K = 4$ rad/s and $\eta_0 = 0.77$ and 0.71. The graphs are presented versus the starboard angle (from 0° to -180°) and versus the corresponding pseudo-incidence (from 0° to 180°).

3.1 Position of the zero-torque point

As defined in section 2.3.1, L_{ip} is the algebraic distance between I , the centre of the blade, and P , the point where the torque is zero. To analyse the evolution of this point, the quantity $d_{ip} = L_{ip} / (0.5c)$ is plotted in Fig. 5 which shows the evolution of d_{ip} for the flat blade and the spherical blade.

The complexity of the flow results in an oscillatory signal but it is possible to observe a trend. During the rowing stroke, the point P migrates from the outer edge of the blade towards the shaft and does not go beyond the middle of the blade at the end of the

Table 1 Characteristics of the tested blades

Blade characteristics	pal0bis flat blade	pal1 spherical blade
Chord length c (m)	0.300	0.283
Height H (m)	0.140	0.1275
Aspect ratio	0.466	0.45
Projected area (m ²)	0.0420	0.0361
Transverse and longitudinal curvature (m)	0	1
Angle γ (deg) shaft-blade chord	0	-5

stroke ($\theta = -130^\circ$). The explanation is due to two conjugated effects: the migration of the point where the hydrodynamic force is applied on the blade and the influence of a pure moment on the blade generated by the difference in the velocities of the blade tips due to the rotation. The pure moment is probably always positive, thus the point P is located towards the outer edge. This is confirmed by the fact that at $\theta = -90^\circ$, where the application point is near the middle of the blade, the point P is located at a quarter of the chord from the outer edge. The ratio between the pure moment and the moment of hydrodynamic force increases with the reduced frequency. Thus, the rotation is more significant if the coefficient η_0 is high and then the point P is nearer the outer edge. In the second part of the stroke, when the inner edge becomes the leading edge, the application point of the force migrates to the shaft but never goes beyond the middle of the blade.

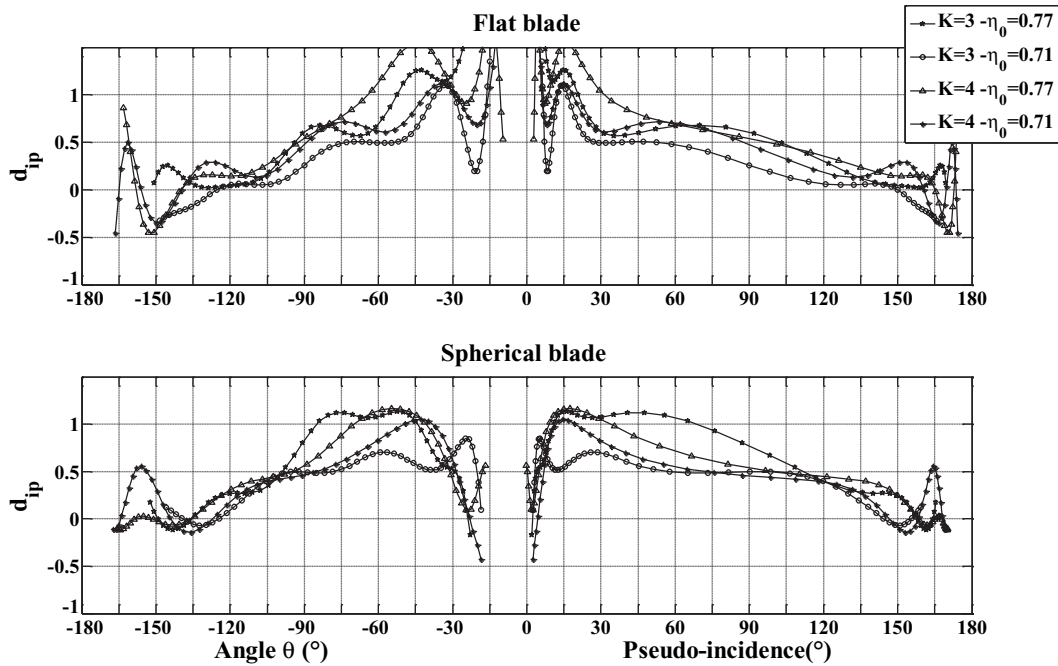


Fig. 5 Evolution of d_{ip} , the ratio of the zero-torque point position \bar{P} to $c/2$, the half chord of the blade. When $d_{ip} = 1$, P is located at the outer edge of the blade

Looking closely at the difference between the flat and spherical blades, it can be observed that the displacement of P is smaller for the spherical blade at the beginning of the tested strokes. The angle $\gamma = -5^\circ$ of the chord to the shaft reduces the incidence of the flow on the blade and the curvature effect probably leads to a more central position of the application point. It is also possible that the smaller incidence at the leading edge and the curvature slightly decrease the pure moment.

However, considering the swing amplitude of a real stroke, the displacement of the point P is similar for the two blades.

The influence of the position of P on the efficiency is shown in Fig. 6 where $\eta_p = 1 - (L_{ip}/Le)$ is plotted versus the swing angle and the pseudo-incidence.

In order to deduce the forces on the oar lock or on the hands of the rowers, a practical result is that it is a little more accurate to approximate $M_z = (\mathbf{OP} \times \mathbf{F}) \cdot \mathbf{e}_{zO}$ by $M_z = [(Le + c/4)\mathbf{e}_{xm} \times \mathbf{F}] \cdot \mathbf{e}_{zO}$ rather than by $M_z = [Le\mathbf{e}_{xm} \times \mathbf{F}] \cdot \mathbf{e}_{zO}$, as is commonly done to calculate the moment of the hydrodynamic force.

3.2 Direction of the hydrodynamic forces

In Fig. 7, the evolution of the angle β between the hydrodynamic force and the normal to the shaft is presented. Although this quantity fluctuates, a trend can be clearly seen. The component η_f of the oar efficiency is $\eta_f = 1 + \tan \beta / \tan \theta$. According to the reference frame for the angle (Fig. 2), the angle β is

favourable for propulsion and efficiency ($\eta_f > 1$) when it is negative for $\theta = [0^\circ, -90^\circ]$ and positive for $\theta = [-90^\circ, -180^\circ]$. Notice that η_f is always unity when $\theta = -90^\circ$. Figure 6 shows a comparison of η_f for the flat and spherical blades. For the flat blade (with $\gamma = 0$), Figure 6 illustrates that the direction of the hydrodynamic force is always unfavourable for overall efficiency. For the spherical blade ($\gamma = -5^\circ$), the force direction is favourable for efficiency between $\theta = -45^\circ$ and $\theta = -90^\circ$, that is to say, during the first part of the stroke. This difference comes from the angle of the blade chord to the shaft ($\gamma = -5^\circ$) which directly rotates the hydrodynamic force towards the direction of advance. It can also be observed that a decrease in the β angle for the spherical blade, compared to the flat blade, is greater than γ , and it may be supposed that the γ angle and the curvature also have a favourable effect on lift. They reduce the local incidence at the leading edge and probably give a longer efficient lift effect at the beginning of the stroke. However, the consequence for the spherical blade is that the β angle is unfavourable during the second part of the stroke for $\theta = [-90^\circ, -140^\circ]$. Notice that for real oars, the deformation induces a rotation of the blade which has a similar effect on the hydrodynamic force orientation.

A practical conclusion of the effect of the hydrodynamic force orientation is that it is possible, according to the technique of the rowers, to improve

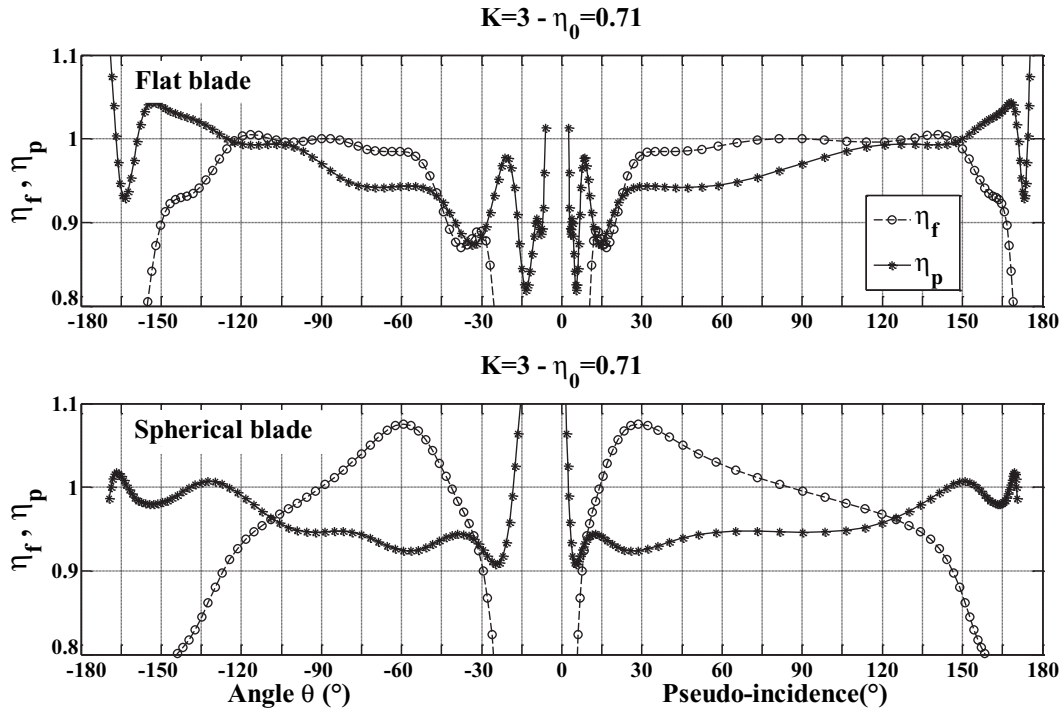


Fig. 6 Dependence of the efficiency coefficient η_p on the zero-torque point and the dependence of the efficiency coefficient η_f on the direction of the hydrodynamic force to the oar shaft

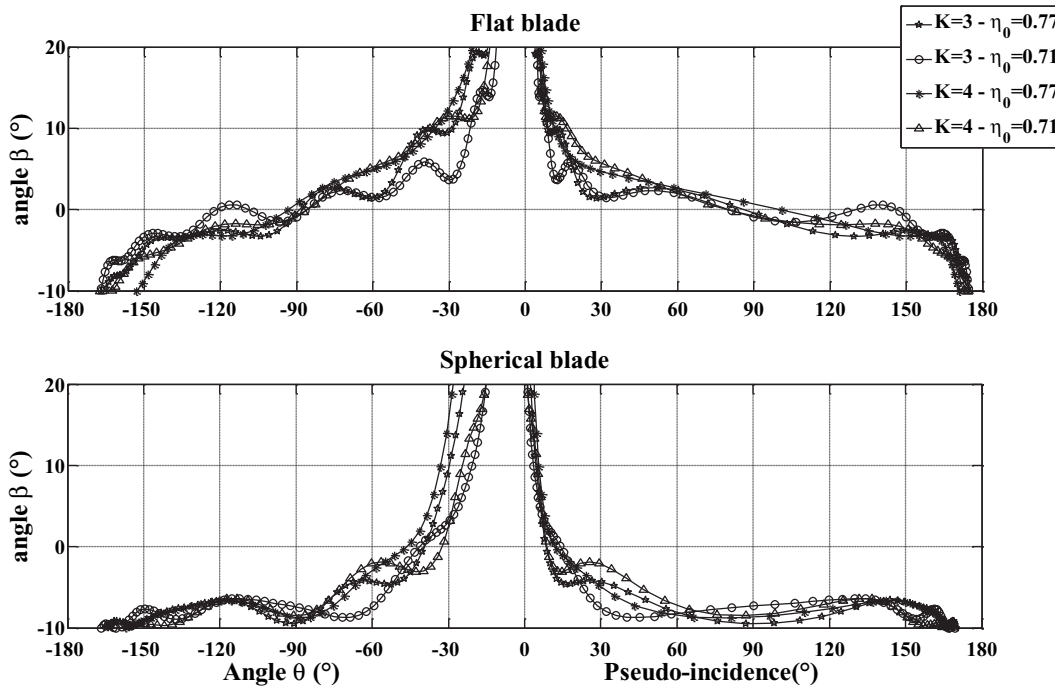


Fig. 7 Angle between the hydrodynamic force on the blade and the oar shaft

the efficiency at the beginning or at the end of the stroke by acting on the curvature and on the γ angle, but it seems difficult to make improvements in both sectors. There is no effect on the efficiency during the

central part of the stroke where the hydrodynamic force is the greatest. Another conclusion is that at least the angle of the chord must be taken into account when modelling the hydrodynamic forces on blades.

3.3 Drag and lift coefficients

Drag and lift coefficients can be expressed by the following relationships

$$C_D = F_D / 0.5 \rho S_p V_p^2 \quad \text{and} \quad C_L = F_L / 0.5 \rho S_p V_p^2 \quad (9)$$

when $V_p^2 = V_t^2 + V_n^2 = V_b^2 \cos^2 \theta + (Le\theta - V_b \sin \theta)^2$. Figure 8 shows the results for the flat blade. Because they are more representative of the influence of the incident flow, the graphs versus the pseudo-incidence angle are more exploitable than the graph versus the oar swing angle.

The C_D graphs are quasi-symmetrical about $\alpha = 90^\circ$ and $C_{D \max}$ is close to 90° . The C_L graph is quasi-antisymmetrical about $\alpha = 90^\circ$. For $K = 3$ rad/s, $C_{L \max}$

and $C_{L \min}$ are close to 45° and 135° whereas for $K = 4$ they are slightly translated by 5° towards 90° .

At the beginning of the stroke, at an incidence angle up to 10° , it can be seen that the blade is working as a lifting surface with no stalled flow, but it is out of a real stroke.

As a first approximation, the shape of the $C_D(\alpha)$ and $C_L(\alpha)$ graphs suggests adopting a kind of first harmonic for modelling the coefficients. This leads to a simple form, with only two coefficients, which will be called 'model 2'

$$\begin{aligned} C_D &= 0.5 C_{D \max} (1 - \cos 2\alpha) \quad \text{and} \\ C_L &= C_{L \max} \sin 2\alpha \end{aligned} \quad (10)$$

The modelling seems to be satisfactory for all tested cases. However, for the two typical examples shown

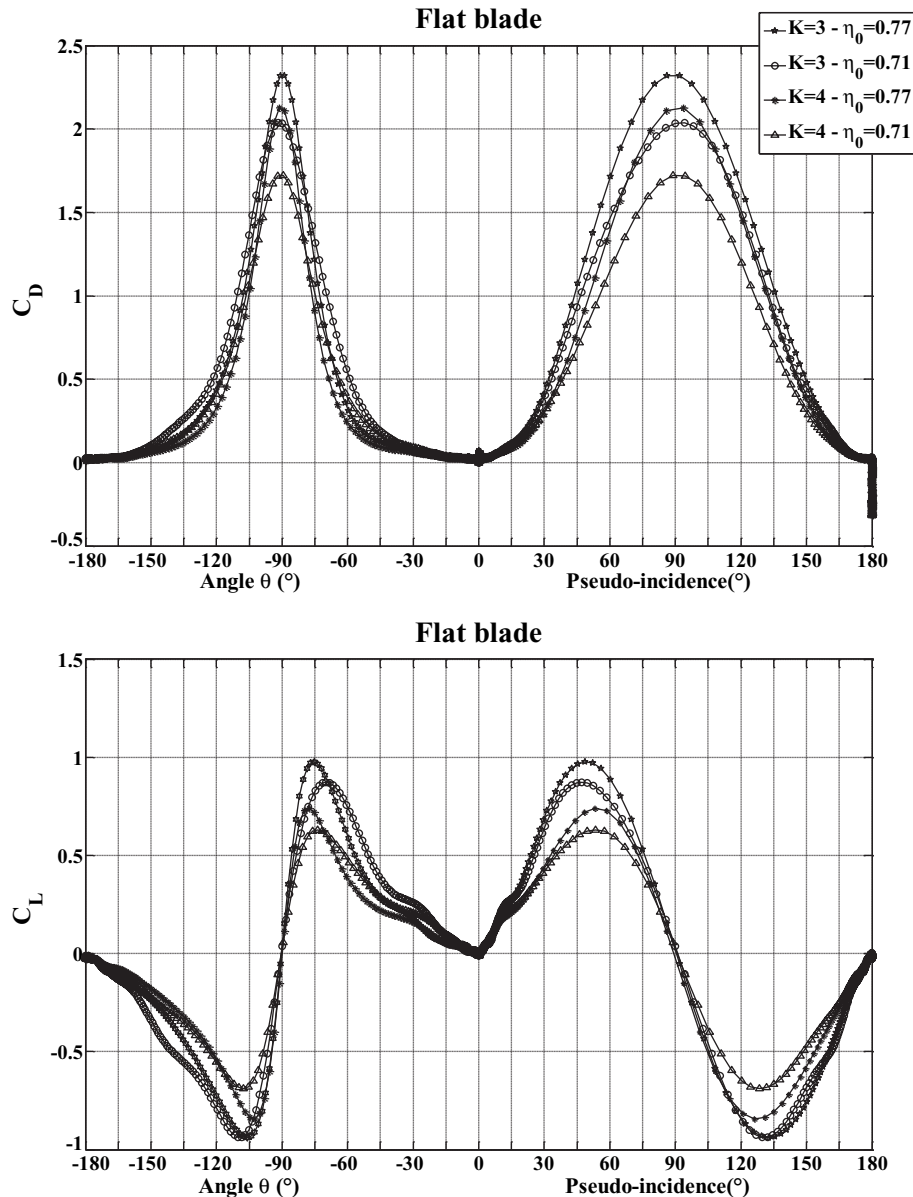


Fig. 8 Drag and lift coefficients

in Fig. 9, it can be observed that model 2 overestimates the coefficients at the beginning and at the end of the stroke.

The normal and tangential forces about the blade chord are related to drag and lifting force by the following relationship

$$\begin{aligned} F_{nc} &= F_D \sin \alpha + F_L \cos \alpha \\ F_{tc} &= -F_D \cos \alpha + F_L \sin \alpha \end{aligned}$$

Hence

$$\begin{aligned} F_{nc} &= 0.5\rho S_p V_p^2 \left[\frac{C_{D \max}}{2} (1 - \cos 2\alpha) \sin \alpha \right. \\ &\quad \left. + C_{L \max} \sin 2\alpha \cos \alpha \right] \\ F_{tc} &= 0.5\rho S_p V_p^2 \left[-\frac{C_{D \max}}{2} (1 - \cos 2\alpha) \cos \alpha \right. \\ &\quad \left. + C_{L \max} \sin 2\alpha \sin \alpha \right] \end{aligned}$$

As $V_{nc} = V_p \sin \alpha$, then

$$\begin{aligned} C_{nc} &= F_{nc} / 0.5\rho S_p V_{nc}^2 \\ &= \left[C_{D \max} + 2C_{L \max} / (\tan \alpha)^2 \right] \sin \alpha \\ C_{tc} &= F_{tc} / 0.5\rho S_p V_{nc}^2 = (2C_{L \max} - C_{D \max}) \cos \alpha \end{aligned} \quad (11)$$

This model gives $C_{nc \pi/2} = C_{D \max}$ and $C_{tc} = 0$ when $\alpha = \pi/2$.

The assumption that the hydrodynamic force is perpendicular to the blade chord whatever the incidence angle is verified only if $C_{D \max} = 2C_{L \max}$. Figure 8 shows that this is not the case. The ratios $C_{D \max} / C_{L \max}$ and $C_{D \max} / C_{L \min}$ are always greater than two and are approximately 2.2.

3.4 Comparison of current modelling of forces on oar blades

Looking now at the basic model suggested by Wellicome [8], i.e. $F_{nc} = 0.5\rho S_p V_{nc}^2 C_{nc}$, where $C_{nc} = C_{nc \pi/2} = C_{D \max}$ and $F_{tc} = 0$ ($\forall \alpha$), this last assumption requires that $C_{D \max} = 2C_{L \max}$ and then

$$\begin{aligned} F_{nc} &= 0.5\rho S_p V_{nc}^2 C_{D \max} \left(1 + \frac{1}{\tan^2 \alpha} \right) \sin \alpha \\ &= 0.5\rho S_p V_{nc}^2 C_{D \max} \times \frac{1}{\sin \alpha} \end{aligned}$$

One could think that the basic model would be improved for the whole stroke by taking into account the pseudo-incidence in this way. This is not the case because the basic model is not physically coherent.

The current models of forces on oar blades are now compared, that is to say

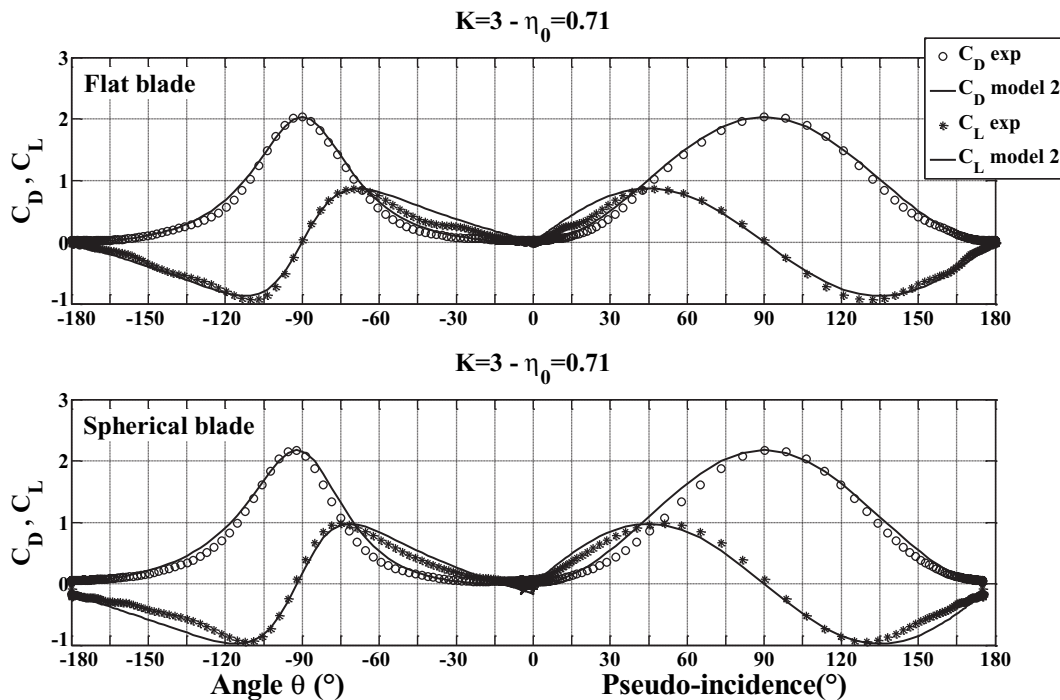


Fig. 9 Comparison of model 2 with measured data for drag and lift coefficients

Model 1 (basic model)

$$\begin{aligned}
 F_{nc} &= 0.5\rho S_p V_{nc}^2 C_{Dmax} \\
 F_{tc} &= 0 \quad (\forall\alpha) \\
 F_x &= -F_{nc} \sin(\theta + \gamma)
 \end{aligned}
 \tag{12}$$

Model 2

$$\begin{aligned}
 F_{nc} &= 0.5\rho S_p V_{nc}^2 \left[C_{Dmax} + 2C_{Lmax}/(\tan\alpha)^2 \right] \sin\alpha \\
 F_{tc} &= 0.5\rho S_p V_{nc}^2 (2C_{Lmax} - C_{Dmax}) \cos\alpha \\
 F_x &= F_{tc} \cos(\theta + \gamma) - F_{nc} \sin(\theta + \gamma)
 \end{aligned}
 \tag{13}$$

Figure 10 shows that model 1 underestimates the propulsive force whereas model 2 overestimates it. However, model 2 better represents the shape of the graph and the influence of the γ angle of the blade chord to the shaft. For both models, it is important to consider the flow and the forces along the axes of the chord. However, the differences between the measured data and the propulsive forces given by model 2 are greater than would be expected with the model of the drag and lift coefficients.

Figure 10 shows that the tangential efforts at $\theta = 0^\circ$ and $\theta = -180^\circ$ are not negligible. Friction effects are not sufficient to explain this fact; there is also a form effect due to the square shape of the leading edge and the immersed part of the shaft.

It would be possible to obtain a better model for the coefficients C_D and C_L by using mathematical fitting but it is risky to do that without verifying the physical consistency of the modelling according to the shape of the blade, the working parameters, and the complex flow around the blade.

It can be noticed that model 2 enables the moment of the hydrodynamic force to be calculated better even when the blade has an angle γ to the shaft and when the oar is no longer considered as rigid.

To conclude this part, it appears that the coefficients C_{Dmax} and C_{Lmax} are the most important quantities to be evaluated for modelling the propulsive force. The problem is now to calculate these coefficients according to the working parameters of the oar.

3.5 Maximum value of drag and lift coefficients (C_{Dmax} , C_{Lmax})

Figure 11 shows that C_{Dmax} and C_{Lmax} depend on η_0 and K , in other words, on the law of incidence variation and on the maximum rate of oar rotation. In order to highlight the influence of unsteadiness, these coefficients are presented against the reduced frequency.

For the neutral kinematic, $V_n = (Le\dot{\theta}_{max} - V_b) = 0$, then $\eta_0 = 1$ and $f_r = \infty$. The minimum value of the reduced frequency is $f_r = c/Le$ for an advance number $\eta_0 = 0$, that is to say a boat velocity $V_b = 0$.

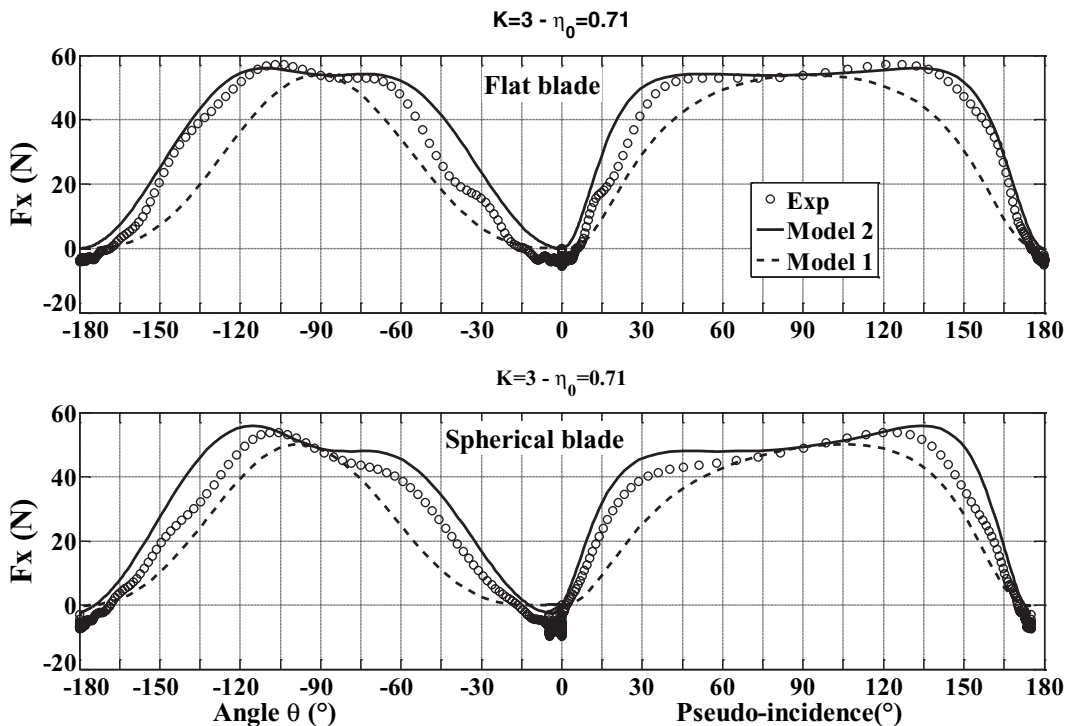


Fig. 10 Comparison of measured propulsive force F_x with the different models

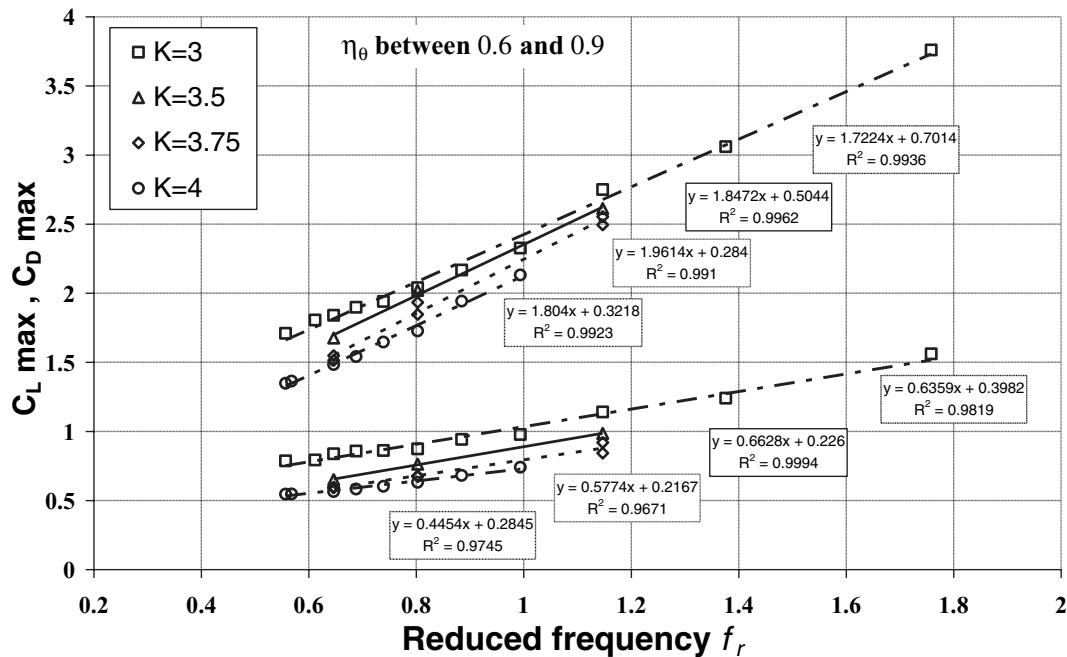


Fig. 11 Maximum lift and drag coefficients versus reduced frequency for the flat blade

In the range of the advance numbers which have been tested, both coefficients vary almost linearly with f_r for a given value of the parameter K . The slopes of the plots are similar and, for a given reduced frequency (or advance number), they increase when the maximum rate of rotation K decreases. It is not easy to compare these with the results of Kinoshita and Kobayashi [1], because the reduced frequency which they used is based on a uniform incident velocity and the reduced frequency is zero for the steady case. With the present approach, the reduced frequency is based on the normal velocity and on a particular kinematic law, thus the steady motion cannot be obtained but only a pure rotation with $V_b = 0$. However, a similar conclusion is highlighted concerning the influence of unsteadiness on propulsive coefficients.

There are two areas in which these kinds of graphs can be exploited. First, for estimating the forces on the oars in tests on water when only the movement of the oars and the boat velocity are measured. In this case, all the working parameters are known and the coefficients can be evaluated directly on the graphs. Second, in simulations when the swing angle is imposed. In this case, the maximum rate of rotation K is known but the advance number and the reduced frequency are not *a priori* known because the velocity of the boat is calculated by the simulator. The values of C_D and C_L have to be adjusted from one cycle to the next, according to their linear variation, until convergence is obtained.

4 CONCLUSIONS

The tests which were analysed relate to a simplified kinematics of the oars. It will thus be necessary to check if these results remain valid for real kinematics, particularly with a variation in boat velocity. Exploring the influence of the immersion of the blades on the propelling coefficients remains to be done.

However, this study highlights the significant parameters which will enable the modelling of the hydrodynamic force to be improved. The results confirm the influence of unsteadiness on the forces and also that of the maximum rate of rotation, related to the Froude number and thus to the free-surface effects. In addition, the impact of the shape of the blade and its orientation on the shaft is demonstrated.

A comparison of the models usually used shows that the model using the lift and drag coefficients overestimates the propulsive component of the hydrodynamic force. However, as it seems better for following the physics of the phenomena than the basic model, which is only based on the coefficient of the normal force, it may be more easily improved by mathematical adjustment. Nevertheless, the maximum values of the drag and lift coefficients seem to be the key parameters for modelling the forces on oars. The trend of their dependence versus the reduced frequency and at the maximum rate of rotation suggests that they could be estimated in a simple way knowing the working parameters.

In the future, the reduced frequency will be used to analyse tests on real oars carried out in a towing

tank using the same method. It will then be justified to have recourse to a fitting of the models since one will be interested in oars with known characteristics which are used for simulations and for tests on water.

CFD calculations must be performed to validate the models for real movements, since CFD calculations are not dependent on the simplifications imposed by the experimental approach and there are no constraints on the kinematics.

ACKNOWLEDGEMENTS

This study was carried out within the framework of a research programme on rowing, jointly developed by the French Rowing Federation (FFSA), the Ecole Centrale de Nantes (ECN), and the Ecole Nationale de Voile et des Sports Nautiques (ENVSN) and supported by the French Ministry of Sports (MSS) and the 'Région des Pays de la Loire'.

© Authors 2010

REFERENCES

- Kinoshita, T. and Kobayashi, H.** Improving rower motion and rowing equipment by using rowing velocity prediction program with estimated hydrodynamic load acting on an oar blade. *Int. J. Small Craft Technol. (RINA)*, 2004, **146**, 16–26.
- Caplan, N. and Gardner, T.** Modelling the influence of crew movement on boat velocity fluctuations during the rowing stroke. *Int. J. Sports Sci. Engng*, 2007, **1**(3), 165–176.
- Leroyer, A., Barré, S., Kobus, J. M., and Visonneau, M.** Experimental and numerical investigations of the flow around an oar blade. *J. Marine Sci. Technol.*, 2008, **13**, 1–15.
- Doi, Y., Ueda, T., Mori, K. H., and Nimomiya, S.** Study on rowing simulation and its application to evaluate oar size and rowing pattern (in Japanese). *J. Soc. Naval Arch. Jpn*, 1999, **186**, 89–96.
- Caplan, N. and Gardner, T. N.** A fluid dynamic investigation into the Big Blade and Macon oar blade designs in rowing propulsion. *J. Sports Sci.*, 2007, **25**, 643–650.
- Barré, S. and Kobus, J. M.** New facilities for measurement and modelling of hydrodynamic loads on oar blades. In *Proceedings of the Second International Conference on The Engineering of Sport*, Sheffield, 1998.
- Barré, S.** *Etude expérimentale des systèmes de propulsion instationnaire. Application aux palettes d'aviron.* PhD Thesis, Université de Nantes et Ecole Centrale de Nantes, 1998.
- Wellicome, J. F.** Some hydrodynamic aspects of rowing. In *Rowing, a scientific approach* (Eds J. G. P. Williams and A. C. Scott), 1967, pp. 22–63 (Kaye and Ward, London).

APPENDIX

Notation

A	application point of the force
c	blade chord
C_D, C_L	drag and lift coefficients
C_n	normal force coefficient (to the shaft)
C_{nc}	normal force coefficient (to the chord of the blade)
e	scale of the blade
(e_{xb}, e_{yb}, e_{zO})	frame of reference linked to the towing tank carriage or boat or dynamometer
(e_{xm}, e_{ym}, e_{zO})	frame of reference linked to the oar shaft
f_r	reduced frequency
F	hydrodynamic force on the blade
F_D, F_L	drag and lift forces along the axis of the incident velocity
F_n, F_t	measured force components along the shaft axis
F_{nc}, F_{tc}	measured force components along the blade chord axis
Fr_n	Froude number calculated at $\theta = -90^\circ$
F_x, F_y	measured force components along the dynamometer axis
I	reference point (centre of blade surface)
K	kinematic parameter, maximum rate of rotation
Le	outboard lever, the distance between the rotation axis and the centre of the blade
L_{ip}	algebraic distance between I and P in the horizontal plane
m	pure moment acting on the blade
M_O, M_P	moments applied to the blade
M_z	component of the hydrodynamic torque applied about e_{zO} (measured torque)
O	origin of the reference frame
P	position of the point where the torque is zero
S_p	projected blade area
V_b	boat velocity (or towing tank carriage velocity)
V_p	relative velocity module of the water at the reference point of the blade
(V_n, V_t)	component of velocity along the shaft axis
α	pseudo-incidence angle (angle between the absolute velocity of the characteristic point of the blade and the blade chord direction)

β	angle between the hydrodynamic force and e_{ym} (normal to the oar shaft)	η_p	efficiency coefficient; depending on the position of the zero-torque point
γ	angle between the blade chord and the shaft	η_o	advance number or main component of efficiency; depending on the oar movement
η	instantaneous propulsive efficiency of the oar alone	θ	angular position between the shaft and the boat velocity; $\dot{\theta} < 0$ for starboard oar
η_f	efficiency coefficient; depending on the direction of the hydrodynamic force compared to the normal of the shaft	$\dot{\theta}$	oar rotation velocity; $\dot{\theta} < 0$ for starboard oar
		ρ	specific mass of water